Reverse Engineering of Super-Attenuator Vertical Control

Report of an Archaeological Excavation Operation Among the Real-Time Codes of VIRGO

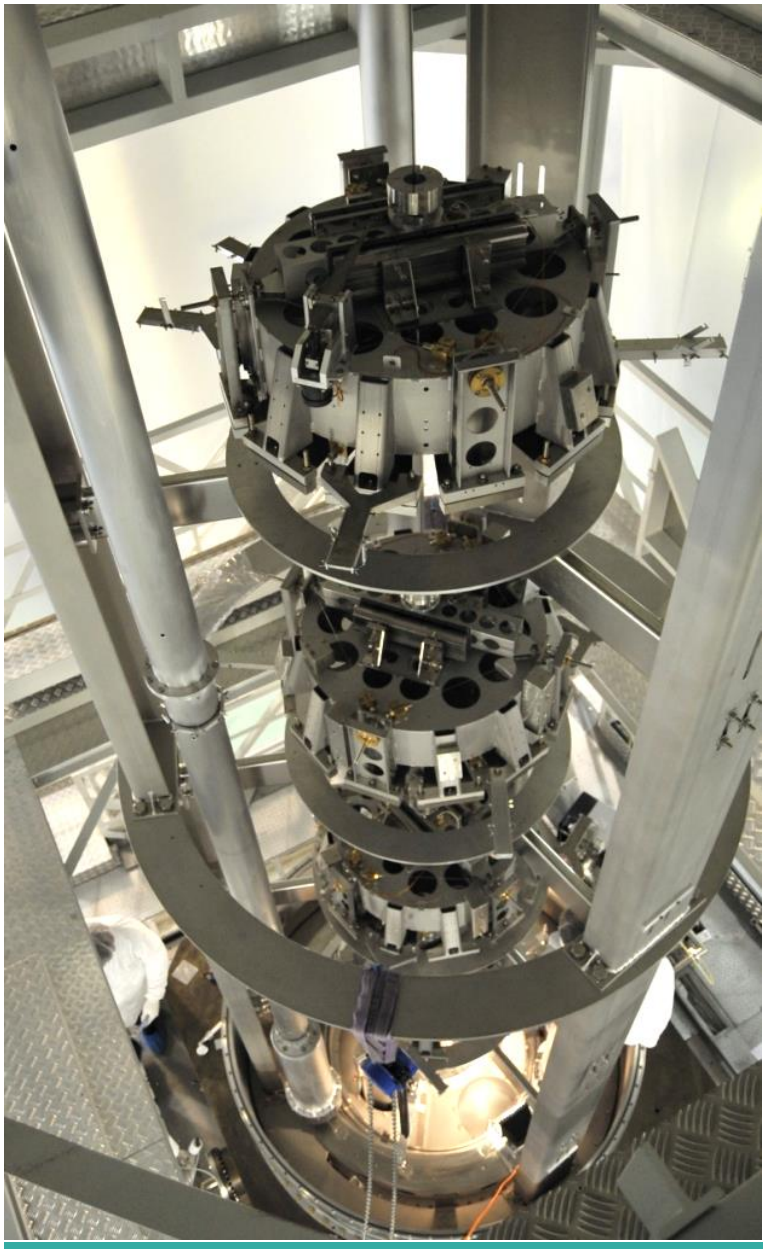

NOVEMBER 9, 2023

Alberto Gennai

INFN PISA
Istituto Nazionale di Fisica Nucleare
Sezione di Pisa

VIRGO

Contents

Introduction

Overview

The absence of project documentation has always been a longstanding issue for VIRGO, particularly within the INFN Pisa group. Year after year, upgrade after upgrade, there has been a genuine accumulation of hardware, software, and various algorithms that would require years of study for a full understanding by those who haven't been directly involved in the detector's development. Starting with one of the simplest examples to grasp, the vertical control of the super-attenuators, we attempt to examine the system in operation by reading the code and endeavouring to provide a correct interpretation for each individual block. This report assumes that the reader has a basic understanding of systems and control theory. Among the references, two of the most renowned books on these topics are cited. [RD1] [RD2].

Reverse Engineering

“Reverse engineering (also known as backwards engineering or back engineering) is a process or method through which one attempts to understand through deductive reasoning how a previously made device, process, system, or piece of software accomplishes a task with very little (if any) insight into exactly how it does so” [RD3].
The algorithms that control VIRGO's super-attenuators are the result of continuous upgrade and adaptation work that began over 25 years ago and has never ceased [RD4]. Unfortunately, the upgrade work is very rarely documented, and there is even less documentation available regarding the project, its implementation, and testing. The only practical way to understand how a given control algorithm operates is by tracing back to the code and attempting to deduce its operations through a posteriori deductive process.

Acronyms

AD	Analog to Digital
DA	Digital to Analog
DDR	Double Data Rate SDRAM
DSP	Digital Signal Processor
GFLOP	Giga Floating Point Operations Per Second
GPP	General Purpose Processor
INFN	Istituto nazionale di Fisica nucleare
LVDT	Linear Variable Differential Transformer
MFLOP	Mega Floating Point Operations Per Second
MicroTCA	Micro Telecommunications Computing Architecture
MIMO	Multiple In - Multiple Out
NE	North End
RAM	Random Access Memory
RD	Reference Document
SDRAM	Synchronous Dynamic Random Access Memory
SISO	Single Input – Single Output

The Super-Attenuator

Plant Description

As is the case with any respectable control system, we begin with a description of our system. The super-attenuators are complex mechanical structures, standing about ten meters tall, and comprised of a cascade of interconnected pendulums. Their purpose is to isolate the optical components, typically mirrors and optical benches, of the laser interferometer used for gravitational wave observation within the VIRGO project from ground vibrations. To give you an idea of the complexity, it's worth noting that a super-attenuator can be described by a model with more than 80 vibrational modes. For the VIRGO experiment, we utilize 10 super-attenuators.

In order to effectively attenuate ground vibrations, the fundamental modes of the super-attenuators should have the lowest possible frequencies. Since the fundamental oscillation mode of a pendulum is determined by the well-known relationship:

$$f_0 = 1/2\pi \sqrt{g/l}$$

where *g* is the acceleration due to gravity and *l* stands for the length of the pendulum. In order to achieve low resonance frequencies in the horizontal plane, pendulums of sufficient length are required.

The term "Super-attenuator" was first introduced in 1987 in the article referenced [RD5]:

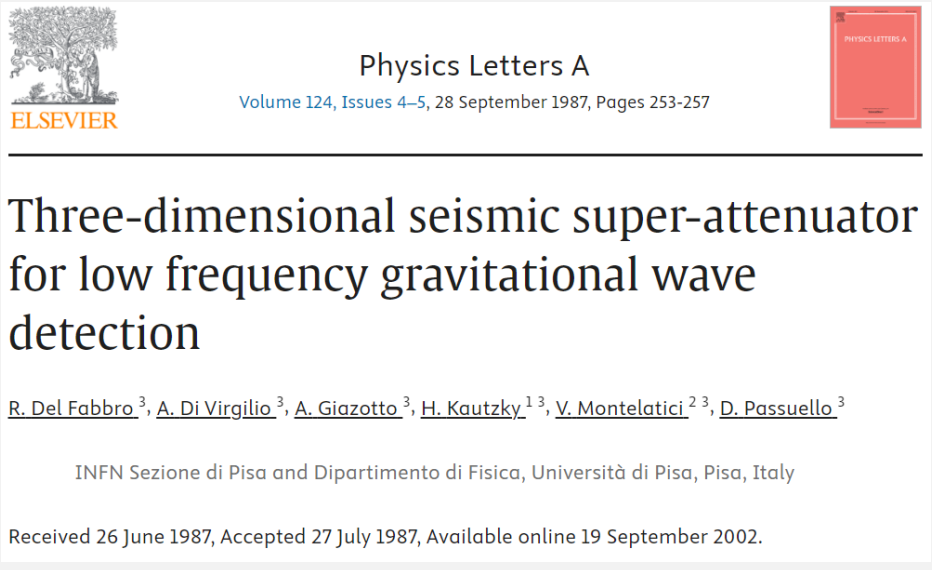

ELSEVIER

Physics Letters A

Volume 124, Issues 4–5, 28 September 1987, Pages 253-257

Three-dimensional seismic super-attenuator for low frequency gravitational wave detection

R. Del Fabbro [3], A. Di Virgilio [3], A. Giazotto [3], H. Kautzky [1 3], V. Montelatici [2 3], D. Passuello [3]

INFN Sezione di Pisa and Dipartimento di Fisica, Università di Pisa, Pisa, Italy

Received 26 June 1987, Accepted 27 July 1987, Available online 19 September 2002.

As recalled in the article where they are first mentioned [RD5], the super-attenuators reduce ground vibrations transmitted to the optical elements suspended from the pendulum chain not only along horizontal directions but also in the vertical direction. In this instance, the resonance frequency that we aim to have as low as possible is that of a mass-spring system, specifically:

$$f_0 = 1/2\pi\sqrt{k/m}$$

where *k* is the spring constant and *m* is the suspended mass. In this scenario, given the mass, the only way to reduce the resonance frequency is to lower the value of the spring constant *k*. In VIRGO, this was achieved by employing an ingenious system of magnetic anti-springs [RD6].

The result of combining low-frequency resonators with a stage of horizontal pre-isolation based on a tall inverted pendulum with normal modes having a period exceeding 30 seconds is a mechanical structure that is far from rigid, rather notably "soft". Very small forces can produce significant displacements: in a pendulum, the low-frequency displacement is determined by the force divided by the pendulum's mass and the square of the resonance frequency:

$$\Delta x = Force/m\omega_0^2$$

The lower the resonance frequency, the greater the displacement for the same applied force. This flexibility means that a super-attenuator cannot stand on its own. Minor assembly inaccuracies and the inability to have absolute control over a fundamental environmental parameter for a mechanical construction—the temperature—further complicates matters. It is impossible to mount a super-attenuator within a small range of its nominal operating point. This aspect introduces an additional task for the control system: the necessity to position and maintain the super-attenuator consistently within a small range around the optimal operating point to ensure the required performance in terms of seismic isolation and positioning of the suspended optics. Without this functionality, the super-attenuator literally sits on its mechanical stops and ceases to operate.

The super-attenuator is not a purely "passive" system: without an active control system, it does not work.

The Control System

General Description

Over the years, the control system for the super-attenuators has continued to evolve Following the initial tests conducted at the INFN laboratories in San Piero a Grado (Pisa in the early '90s, which were inspired by the work of P.R. Saulson in the first half of the '80s [RD8], we soon realized that the complexity of the super-attenuators demanded an equally complex, easily configurable multivariable control system. Right from the beginning, the choice fell on a class of processors specifically designed for this purpose Digital Signal Processors (DSPs).

DSP vs GPP

The differences between "Digital Signal Processors" and "General-Purpose Processors" have played a fundamental role in VIRGO

Today, there's much less discussion about the difference between DSP (Digital Signal Processor) and GPP (General-Purpose Processor). However, during the construction and fine-tuning years of VIRGO, the choice of DSP processors enabled us to achieve performance levels that otherwise would have been unattainable. The operational system at VIRGO since 2015 represents the third generation of DSP-based control systems, transitioning from the first Motorola DSP92002 (up to 2005), to the Analog Devices ADSP-21160N (up to 2014), and since 2015, the Texas Instruments TMS320C6678. The table below illustrates a significant increase in computing power over the years. Notably, the most recent enhancement is linked to the decision to eliminate any analog loop and use the processors for generating reference signals within the 0-100kHz bandwidth.

Year	Processor	Procs per super-att.	Sust. MFLOPS per proc.	Memory
1998	DSP96002	2	20	8kB RAM
2006	ADSP-21160N	4	380	512 MB SDRAM
2015	TMS320C6678	14[1]	60’000	512 MB DDR3

[1] **Number changes from one super-attenuator to another.**

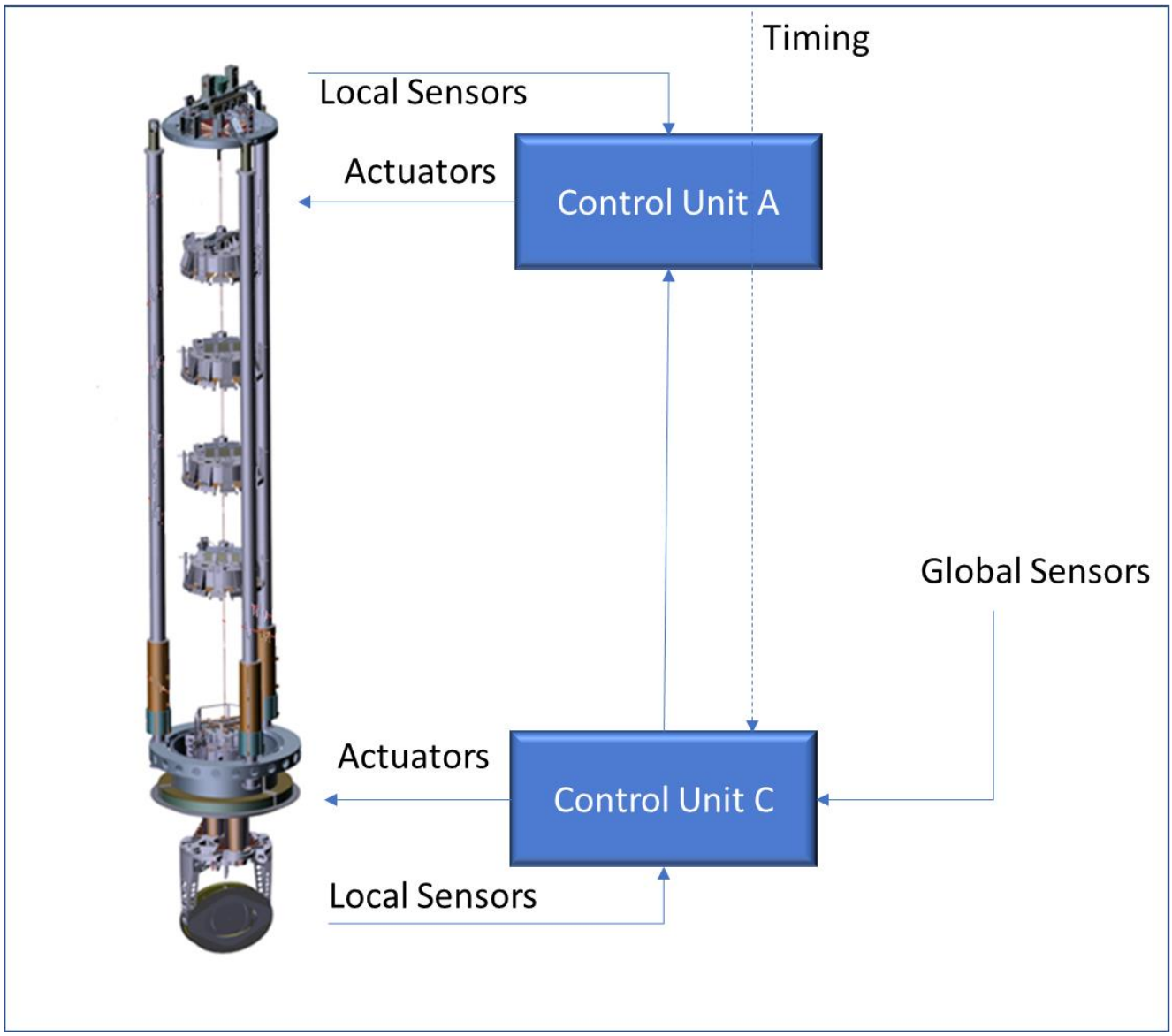

In the previous figure, one of VIRGO's super-attenuators is depicted with its two control units. Each control unit can be equipped with a maximum of 12 DSP processors, although the average number is currently between 6 and 7. Control Unit A, typically indicated by the prefix "Sa" in the names of the processors used, manages the upper part of the super-attenuator. Control Unit C, labeled with the prefix "Sc", handles the lower section and controls the positioning of the suspended mirrors and optical benches.

The form factor used for the 20 local control units of VIRGO is a customization of the MicroTCA standard [RD7]

In this photo, the local control unit used for the upper part of the NE (North End) super-attenuator, which suspends the end mirror of the north arm, is displayed. In this case, there are 6 processors positioned in slots 1, 2, 4, 5, 7, and 11. Each processor interfaces directly through a PCIe link to 6 channels of 24-bit analog-to-digital and 6 channels of digital-to-analog conversion. A critical feature of the system is the complete absence of active electronic components in the vacuum chambers containing the super-attenuators. All the necessary electronics for controlling the upper part are contained within the cage, except for the motor drivers, which are housed in a separate, isolated cage. The black cables are multi-pole conductors that carry analog signals. The red cable to the left is the connection to VIRGO's timing system. Highlighted in orange are two fiber optic links for connecting to other control units and VIRGO's data acquisition system. Each individual processor is connected to the network via a dedicated Ethernet connection, which, through the backplane, reaches the switch placed to the right, immediately next to the power supply unit.

For the control of the whole VIRGO detector we use 135 8-cores processors DSP, capable of 22.4 GFLOPs/core @ 1.4 GHz

Hardware, Software & Algorithms

We can outline the super-attenuator control system with a layered architecture. The control algorithms reside in the application layer, positioned above a dedicated middleware. The software layer conceals the digital system's intricacies and facilitates algorithm development, working as if the control system were continuous-time. In the vast majority of cases, the controllers are designed using the Nyquist technique, imposing general specifications on the open-loop transfer function.

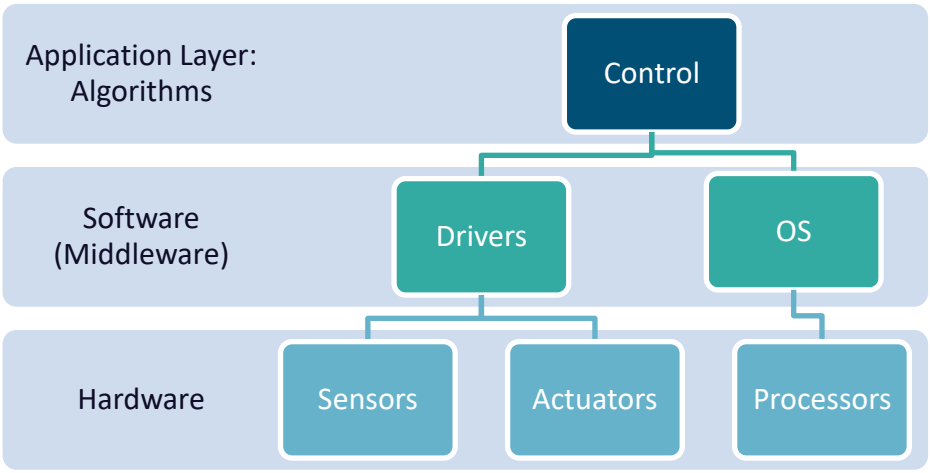

General Requirements

I compiti principali del sistema di controlo dei super-attenuatori sono due:

1. Mantenere i super-attenuatori e gli elementi ottici sospesi in un ***piccolo intorno*** del punto di lavoro che è funzione del tempo.
2. Ridurre l'ampiezza dei picchi di risonanza della meccanica ("Damping") e in generale ridurre ***il più possibile*** le vibrazioni del terreno trasmesse alle ottiche sospese.

Questi compiti devono essere eseguiti inserendo il ***minimo rumore possibile*** in modo che lo spostamento degli specchi sia sempre determinato da rumori fondamentali quali il rumore termico degli specchi stessi e l'errore di misura dell'interferometro

Already from these general specifications, a peculiarity of the control system becomes evident: the lack of set numerical references. The meaning of "small range" is not known a priori, and reducing "as much as possible" in engineering terms is a nonsensical phrase. In the case of VIRGO, these phrases must always be interpreted in light of the current operating state and the noise level (sensitivity) of the entire detector. They might be summarized in a single specification: the super-attenuator control system must move VIRGO's mirrors along trajectories that nullify the error signals along the 'z' direction of

the laser beam and the two angles 'ϑ_y'("yaw") and 'ϑ_x'("pitch") derived from the readings of photodiodes and quadrant detectors.
We are not concerned with reducing the root mean square (rms) value of the errors, but rather aim to decrease their spectral density within a frequency band that is a function of the interferometer's state. Given that this document specifically addresses vertical control, it is essential to note that the VIRGO interferometer is unable to provide an error signal regarding the position along the vertical direction and perpendicular to the laser beam. In this scenario, the error signal must be generated from readings of the super-attenuator and the mirror to which it is attached, taken with local sensors, or by introducing known displacements on the angles θy and θx and measuring the error generated by the interferometer along the z-direction.

An important feature of VIRGO's super-attenuator control system is that disturbance signals such as seismic noise, and where relevant, thermal noise, are typically low-pass signals, characterized by spectral density that decreases with increasing frequency. Specifically, seismic noise, being filtered by the super-attenuator, often exhibits a steep decrease. Considering that the rms displacement is simply the integral of the spectral density, it's easy to imagine that the most significant displacements occur at lower frequencies (with some exceptions). This characteristic allows for what we call "hierarchical control."

Hierarchical control divides the forces to be applied into frequency bands. The actuators acting higher up, farther from the mirrors, are the ones that allow for greater displacements and consequently exhibit more significant noise, which, however, is filtered by the underlying pendulum chain and thus arrives attenuated at the end of the chain. In contrast, the actuators placed lower down, directly on the mirror, are very low-noise actuators (filtered only by the mirror itself) and, as a result, have equally low dynamics. The actuators acting on the "Marionette" - the stage immediately preceding the mirror - are an intermediate case: moderate force and medium noise. It's worth noting that for vertical displacement there are no actuators on the mirror.
.

Hierarchical Control: large forces at low frequency are applied on top of super-attenuator. Small forces at high frequency are applied directly to the mirror and mid-range frequencies are corrected acting on Marionette

Super-attenuator Control

Super-attenuator control is very complex. It is a multi-degree-of-freedom system that is typically strongly coupled. The typical approach used in VIRGO is always the one cited in the 1997 note [RD4], which is to try to transform the multi-input and multi-output (MIMO) system into a set of single-input and single-output (SISO) systems. Once the main modes are decoupled, controllers are implemented by sizing them as continuous-time systems and leaving it to the middleware briefly described in the previous paragraph to convert the system from continuous time to discrete time. Sizing is done by studying the stability of the open-loop gain, which is the product of the controller transfer function and the transfer function of the mechanical system along the degree of freedom under consideration. For the controller design, it is assumed that the system is linear and time-invariant (LTI), an assumption that is valid in small neighborhoods of the operating point.

.

MIMO: Multiple Input – Multiple Output

SISO: Single Input -Single Output

When possible, we always convert a MIMO system in (almost) independent SISO systems

The Vertical Control

Vertical Actuators & Sensors

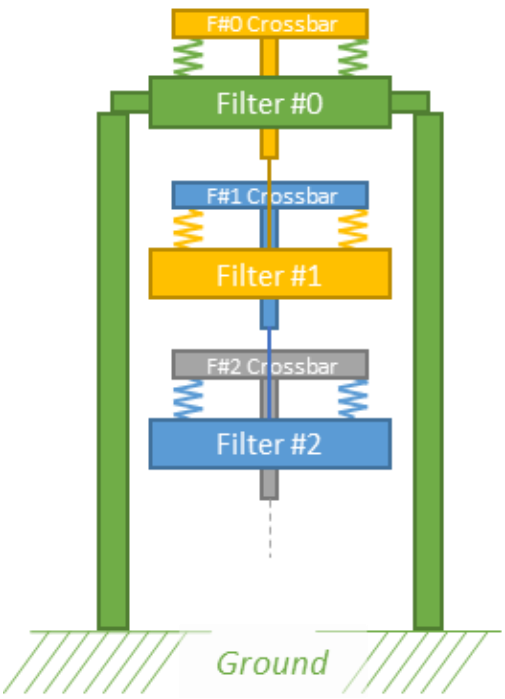

The figure to the side schematically represents the vertical operation of the super-attenuator filter chain. The different colors identify parts that move together. The anti-magnetic springs that act between the cross-bar and the filter, which have the effect of reducing the elastic constant between one filter and the next, have not been represented. Clearly, the diagram can be further simplified as a simple cascade of masses and springs, as has been done in the next figure.

If we want to move a mirror vertically, on which actuators can we act? What sensors can we use?

The actuators with the greatest dynamic range are step-motors. In particular, to set the working position of the mirror along the vertical axis, a motor is used above Filter#0. This motor, called "chiocciolone", is able to move the entire chain starting from Filter#1.

In addition to the "chiocciolone", on each filter except the Marionette, a step-motor adjusts the position of the anti-magnetic spring system, effectively moving the portion of the filter chain below the filter on which the motor is activated. Motors are only used sporadically to adjust the length of the chain and keep the anti-magnetic springs aligned.

The actuators used for linear control in the vertical direction are two voice-coils that can insert a force between Filter#0 and Filter#1. We can refer to the figure on the side. The force F0 between Filter#0 and Filter#1 does not move Filter#0 because it is constrained to move together with the ground (at least indicatively below 10 Hz, the figure diagram is a simplification that assumes all mechanical elements to be infinitely rigid except for the springs explicitly stated in the drawing). F0 therefore moves the entire chain vertically starting from Filter#1.

There is also the possibility of acting with magnet-coil actuators at the level of Filter#7 by inserting forces between the ground and Filter#7 and between Filter#7 and Marionette. These forces are not generally used to correct the position in the vertical direction but only to correct rotations of Filter#7 and Marionette around the x and z axes.

Along the vertical direction, the only linear actuators that we will consider are the two voice-coils that act between the body and the cross-bar of Filter#0 and therefore in fact between Filter#0 and Filter#1, and since Filter#0 is solid with the ground (NB: in the

vertical direction and below about 10 Hz) the force is actually applied between the ground and Filter#1.

Concerning sensors, we have two distinct types. LVDT-type relative displacement sensors measure the relative position between the cross-bar and the body of all filters and therefore, as shown in the figure, measure the relative distance between adjacent filter pairs, up to a constant. In addition, LVDT sensors measure the position of Filter#7 relative to the ground (not shown in the schematic diagram). The second type of sensors used are accelerometers. A pair of vertical accelerometers is installed above the cross-bar of Filter#0 and therefore measures the vertical acceleration of Filter#1.

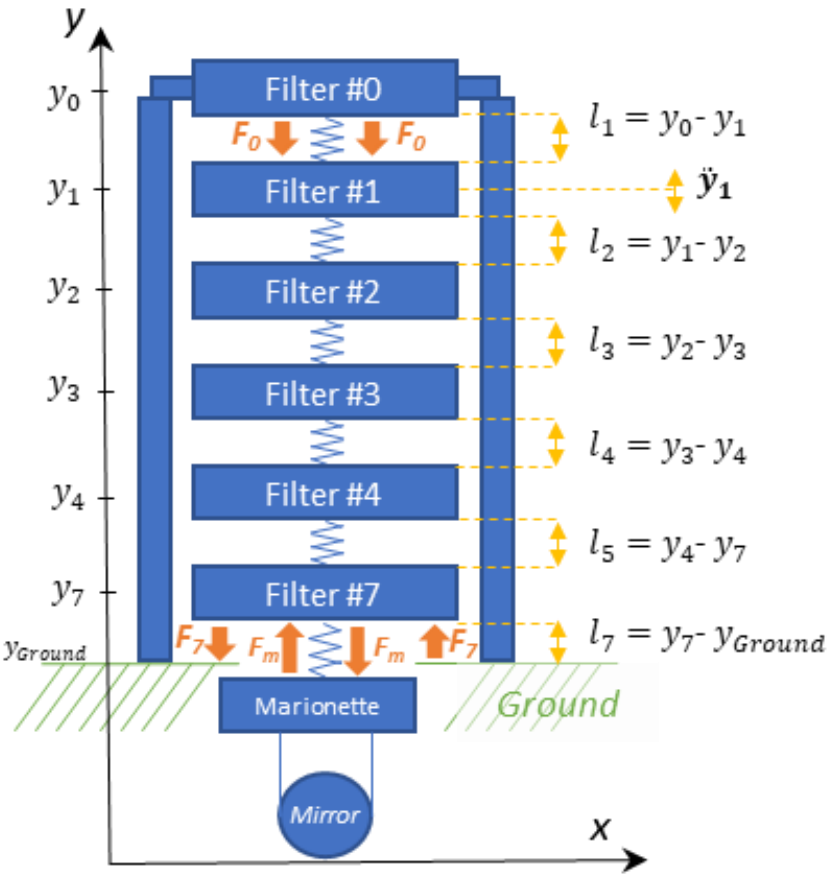

Processors & Processes

As previously mentioned, there are six processors responsible for controlling the upper part of the super attenuator. To identify the processors in use, the following command can be executed from any processor within the EGO farm:

```
gennai@farmn7[~]: grep "host SaNE" /virgoData/Sa/Damping-AdV/setup.dat
host SaNEBRLVDT {
host SaNELVDT {
host SaNECD {
host SaNEAcc {
host SaNEvAcc {
host SaNEVLVDT {
```

Regarding the vertical control, four processors are utilized: SaNELVDT, SaNEvAcc, SaNECD, and SaNEBRLVDT. In some cases, the SaNEVLVDT processor is also employed, but not in the case of the North End super attenuator. The number of cores used among the available 8 per processor varies. All processors utilize 2 cores for inter-processor communication, interfacing with external systems, and reading and writing AD and DA converters. These cores are not user-programmable and implement the "middleware" layer as described earlier. Application-level deployment occurs on cores 1 and 4..

For super attenuator control, core 1 periodically runs a routine at the maximum rated frequency of 320 kHz. Core 4 executes a routine with a typical activation frequency of: 10 kHz for the high part (Sa) and 40 kHz for the low part (Sc). The following figure schematically represents the functions carried out by each processor:

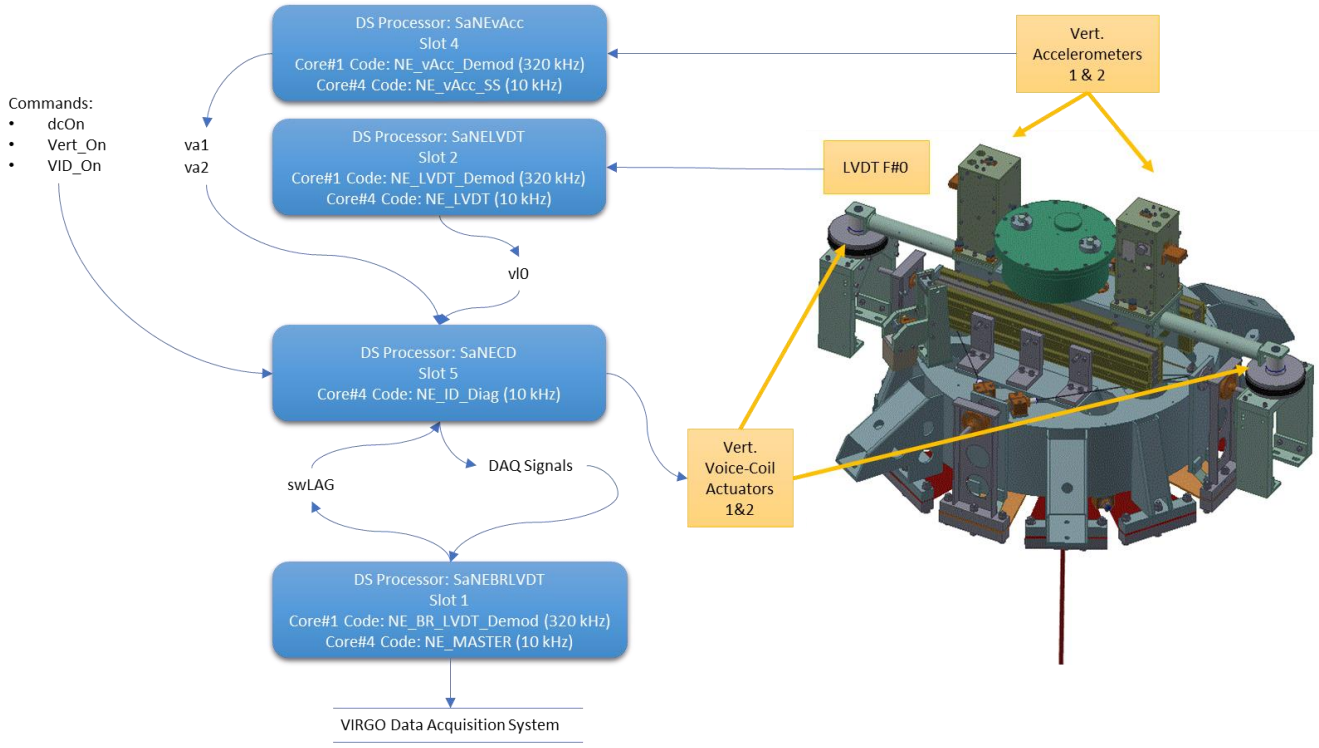

S

- **SaNEvAcc** reads vertical acceleration sensors on the cross-bar, generating va1 and va2 signals transmitted to the SaNECD processor.
- **SaNELVDT** reads LVDT sensors, particularly the LVDT sensor measuring the relative displacement between Filter #0 and its cross-bar, denoted as vl0, transmitted to the SaNECD processor.
- **SaNECD** implements the controller for both horizontal degrees of freedom and vertical control. It determines forces to apply between Filter #0 and its cross-bar using accelerometer readings and LVDT sensor data, employing voice-coils. Additionally, SaNECD receives commands over the network to activate the control system.
- **SaNEBRLVDT** formats data and sends it to the VIRGO data acquisition system.

Detailed algorithms for reading LVDTs and accelerometers are omitted. The accelerometer part is complex due to a feedback loop, given the use of "force balance" type accelerometers. Our focus, however, remains on the vertical control.

The code implementing vertical control lies within NE_ID_Diag, executed by core 4 of the SaNECD processor. The relevant portion of the source code utilized at the application level by users through "damping-adv" application is extracted. The Middleware layer generates executable code from this source code. The language used has not been formalized, with limited and outdated documentation. I've improved code readability by highlighting content within MAT (matrix), SWITCH (SPDT switch), and MIX (multiplier) blocks.

```
gennai@farmn7[~]:damping-adv SaNECD

NE_ID_Diag.hrd (Slot 5)
Input       Output       Filename      GUARD   Gain       Gname      @Frequency  When
ADD         dcOn                       yes     1          F0_DC_ENBL
dcOn        genSw            NULL      no      1          F0_POS_ON
genSw       ID_On            NULL      no      1          F0_ID_ON
genSw       Vert_On          NULL      no      1          F0_VPOS_ON
Vert_On     VID_On           NULL      no      1          F0_VID_ON
ADD         yL0                        no      -260       F0_Y_SET
Slot02_04   vl0              NULL      no      1
Slot04_01   va1              NULL      no      1
Slot04_02   va2              NULL      no      1
vl0         yL               NULL      no      1
va1         va1F       vAcc_Resp1.flt no      -415560              0          after
va2         va2F       vAcc_Resp2.flt no      -380262              0          after
Slot01_04   swLAG            NULL      no      1
 MAT                 vA.mat
{{  va1F         va2F }
 {  0.5          0.5 }            yAcc
 {  1            -1  }}           tcAcc
yL          yLE              NULL      no      1
yL0         yLE              NULL      no      -1
yLE         yLA1       elle75.flt      no      1                    0          after
yAcc        yLA1       acca75.flt      no      2.53e-08             1000       after
yLE         yLA2       elle75.flt      no      1                    0          after
yAcc        yLA2       acca75.flt      no      2.53e-08             1000       after
swLAG       swLA             NULL      no      1          swLA
SWITCH      yLA        yLA12           no      1
```

```
{{   input A       input B       control  }
{     yLA1          yLA2          swLA    }}
yLA         fbyf       yCfull.flt     no      0.075                1          after
yLE         fbyi       yCinit.flt     no      0.02                 1          after
MIX         fbyc       VID_On-fbyf    no      1
{{   input A       input B  }
{    VID_On        fbyf  }}
VID_On      VID_Off          NULL      no      -1
ADD         VID_Off                    no      1
MIX         VcPos      Vert_On-VID_of no      1
{{   input A       input B   }
{    Vert_On       VID_Off   }}
MIX         fbyc       VcPos-fbyi     no      1
{{   input A       input B }
{    VcPos         fbyi    }}
fbyc        fby        intg.flt       no      1                    1          after
MIX         yCorr      dcOn-fby       no      1
ADD         yCorr                     no      0
ADD         tcCorr                    no      0
MAT                    vC.mat
{{  yCorr        tcCorr    }
{   0.95         0.95            coilv1    }
{   1.05         -1.05           coilv2  }}
ADD         coilv1                    no      0
ADD         coilv2                    no      0
coilv1      DAC4             NULL      no      1
coilv2      DAC5             NULL      no      1
va1F        vaF              NULL      no      1
va2F        vaF              NULL      no      0
vaF         Slot01_0c        NULL      no      1
yLE         Slot01_0d        NULL      no      1
yAcc        Slot01_0e        NULL      no      1
coilv1      Slot01_15        NULL      no      1
coilv2      Slot01_16        NULL      no      1
yCorr       Slot01_17        NULL      no      1
```

Filter "filename.flt" descriptions will be covered later in a detailed controller description. The Guardian section, responsible for opening the feedback loop upon detecting abnormal sensor signals, is excluded.

Controller Description

To facilitate understanding of the controller's operation, a Simulink model replicating VIRGO's code behaviour has been created. Transfer functions of LTI blocks in the figure are assumed in a continuous-time control system, with Laplace domain poles and zeros. The Middleware system digitally transforms continuous-time filters to discrete-time filters using bilinear transformation with prewarping.

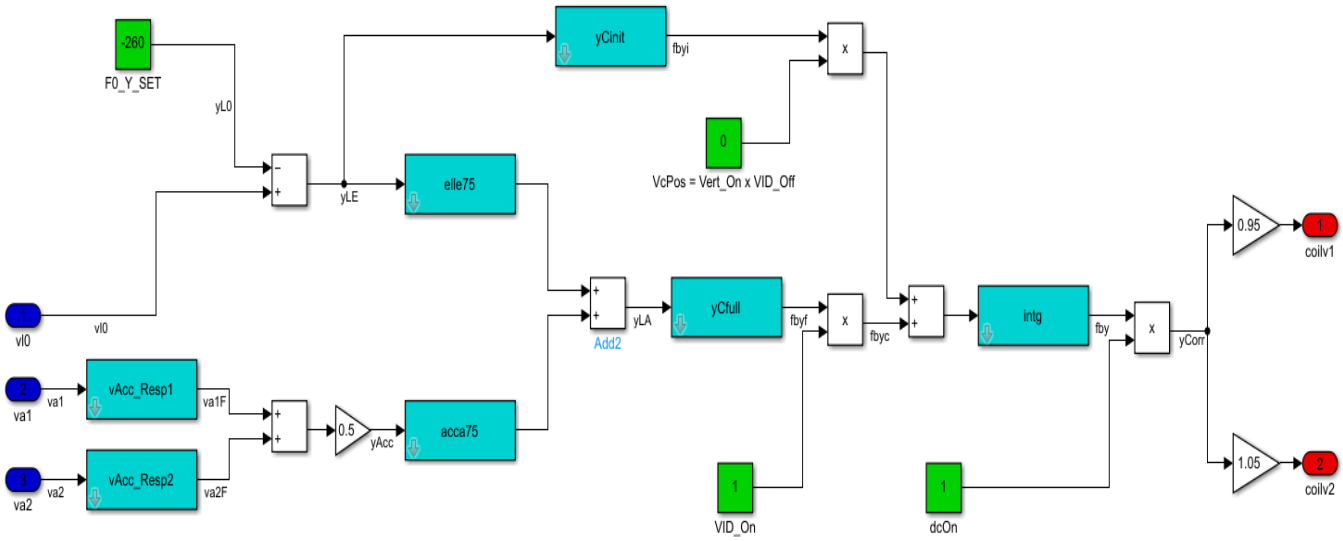

Let's explore how various filters operate in the Simulink scheme.

Let's observe how the various filters are structured according to the Simulink diagram on the left, where the inputs vl0, va1, and va2 are present. For now, let's disregard the branch containing yCinit, as we are examining the scenario in which the control signal VcPos = Vert_On x VID_Off is zero.

The two accelerometer signals are first filtered by vAcc_Resp1 and 2, and then simply averaged. The two accelerometers are symmetrically placed concerning the center of the cross-bar. The sum, divided by two, provides information about the vertical displacement of the cross-bar in Filter#0 and consequently of the body of Filter#1 and the entire chain below. The difference between the two sensors informs about a possible angular displacement of the cross-bar, which might be compensated for using the two voice coils but not in this case. The difference signal is computed by the processor but is not used (tcAcc = va1F - va2F).

The following figure shows the transfer functions of the two LTI (Linear Time-Invariant) blocks named vAcc_Resp1 and vAcc_Resp2. As observed, they consist of a second-order lead-lag network. These filters were introduced when we transitioned the local feedback of the accelerometers from analog to digital. In the analog version, the signal provided by the accelerometers was a wideband acceleration signal (approximately 100 Hz). With the digital version, we limited the acceleration signal bandwidth to the mechanical response of the accelerometer itself.

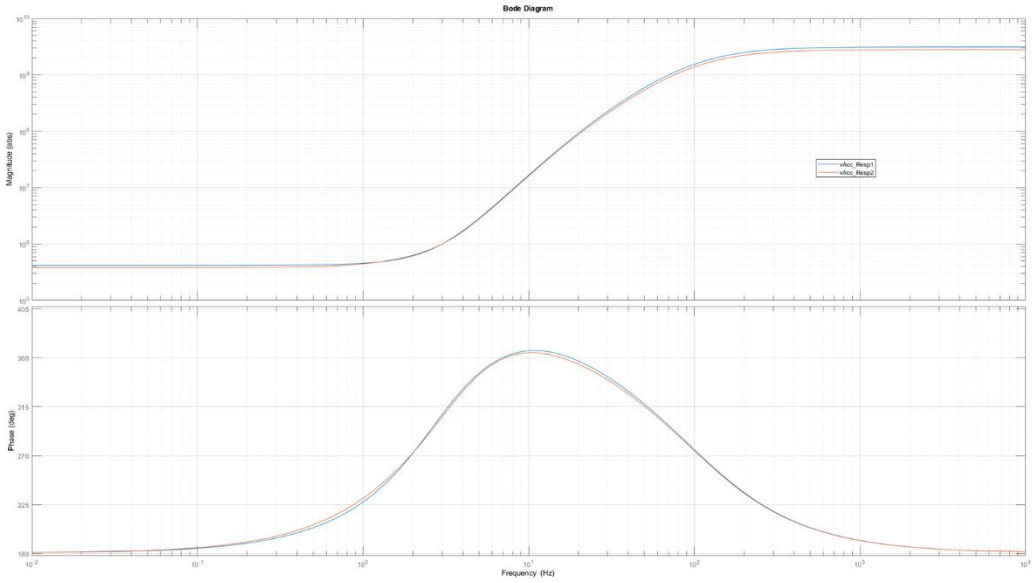

The signals va1 and va2 indeed represent acceleration up to approximately 3 Hz, beyond which the signal is low-pass filtered by the mechanical response. As the downstream control filters were designed for wider-band accelerometers, to simplify the adaptation of the controller to the new accelerometer control, these filters were introduced to compensate for the low-pass action of the accelerometer's mechanics by introducing a pair of zeros around 3 Hz and a pair of poles towards 100 Hz. The differences between the two filters are due to variances in the mechanical response of the two accelerometers. In addition to the double zero and double pole, an additional zero-pole pair introduces a further slight correction in the response.

```
vAcc_Resp1.flt

 Complex zeroes  frequency   2.75              Q       0.6356
 Real    zero    frequency   3.0148
 Real    poles   frequency   100               Q       0.5
 Real    pole    frequency   17.147
```

```
vAcc_Resp2.flt

 Complex zeroes  frequency   3.3958            Q       0.671
 Real    zero    frequency   1.7272
 Real    pole    frequency   14.6479
 Real    poles   frequency   100               Q       0.5
```

The signal yAcc is, therefore, our vertical acceleration signal and, as we have seen, effectively corresponds to the vertical acceleration of Filter#1. Continuing in the scheme, we observe that this signal is filtered by acca75 and added to the output signal from the block elle75, which takes as input the signal vl0, i.e., the readout of the relative displacement between the Filter#0 body and cross-bar, which as mentioned, is the displacement between Filter#0 and Filter#1. The filters elle75 and acca75 form a pair of complementary filters.

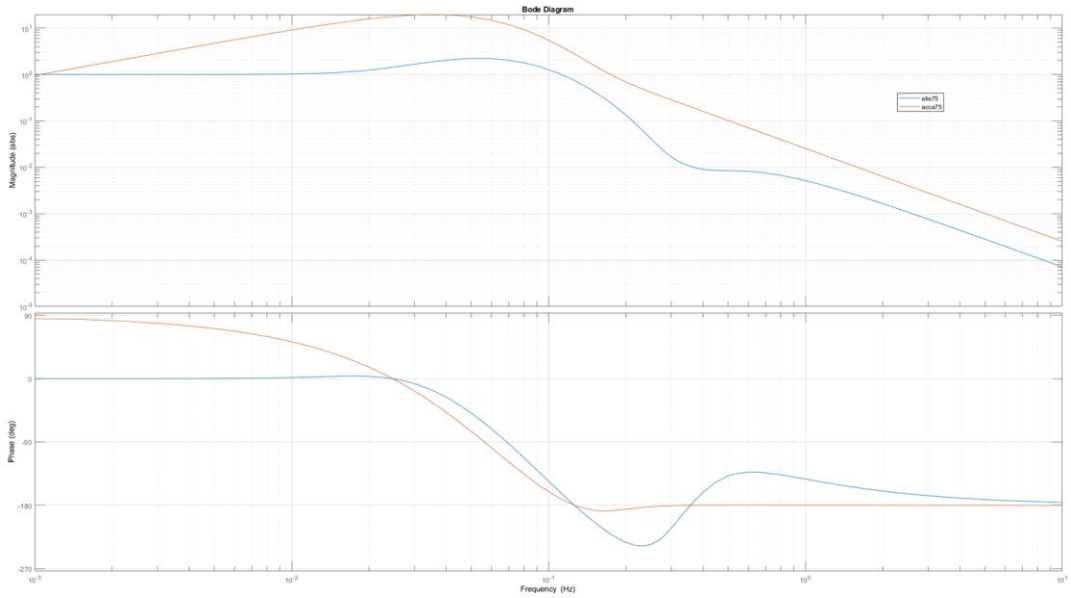


```
acca75.flt
 Real     zero     frequency   0
 Complex  zeroes   frequency   0.1809          Q       1.0752
 Complex  zeroes   frequency   0.3267          Q       0.6177
 Real     pole     frequency   0.075
 Real     poles    frequency   0.075           Q       0.5
 Real     poles    frequency   0.075           Q       0.5
 Real     poles    frequency   0.25            Q       0.5
 Real     pole     frequency   0.3
 Real     zero     frequency   0.4778
```

```
elle75.flt
 Complex  zeroes   frequency   0.0208          Q       0.6433
 Real     pole     frequency   0.075
 Real     poles    frequency   0.075           Q       0.5
 Real     poles    frequency   0.075           Q       0.5
 Complex  zeroes   frequency   0.3             Q       2
 Complex  zeroes   frequency   0.4             Q       1.5
 Real     poles    frequency   0.25            Q       0.5
 Real     pole     frequency   0.3
```

At first glance, they might not seem complementary, but we must consider that the input signals yLE and yAcc represent, the former, a displacement and the latter, an acceleration. Therefore, we can consider yAcc as effectively the second derivative of the displacement of Filter#1. By multiplying acca75 by a transfer function that behaves like s^2 in the region

of interest, we obtain the following Bode plot where it's clearer that the two filters are complementary, elle75+acca75=1, in the region of interest where we expect the open-loop transfer function to have a gain greater than 1.

The calculation of the complementary filter is done using what we refer to as the 'Passuello Polynomials': starting from a Butterworth polynomial of order n, $P_n(s)$, we obtain two polynomials $L_m(s)$ and $H_k(s)$ such that $P_n(s) = L_m(s) + H_k(s)$, where $L_m(s)$ contains the m lower-degree terms and $H_k(s)$ contains the k higher-degree terms (m+k=n). The filters obtained by $L_m(s)/P_n(s)$ and $H_k(s)/P_n(s)$ are one low-pass and one high-pass, and their sum is always equal to 1.

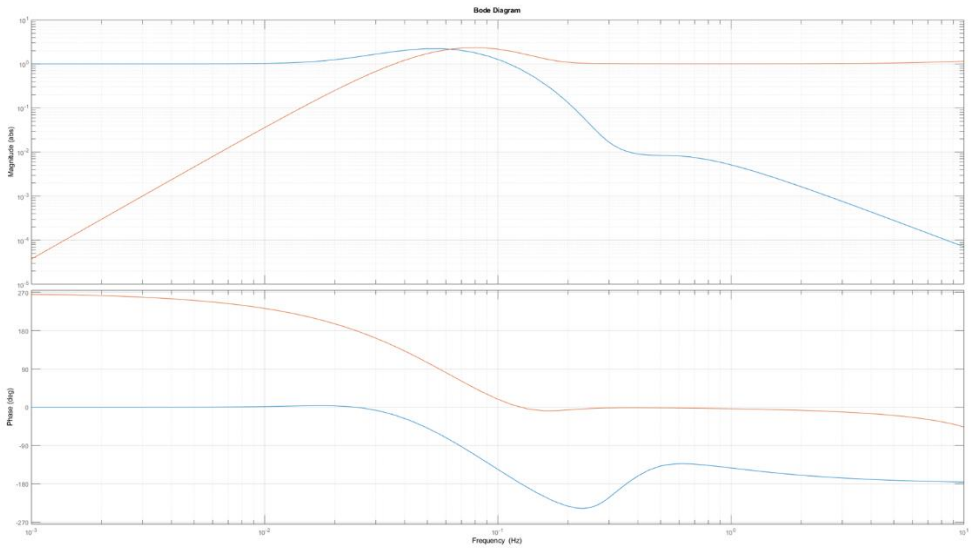

With this operation, we obtain a signal, yLA, proportional to the position of Filter#1. The particularity lies in the low-frequency part obtained from the LVDT sensor reading, given by *l1(t) = y1(t) - y0(t)*, where *y0* represents the position of Filter#0's body, which, within the frequency range of interest, is fixed to the ground. Therefore, we can interpret the signal *l1(t)* as a measurement of *y1(t)* 'contaminated' by vertical ground vibrations. At higher frequencies, *yLA* is derived by integrating twice the accelerometer signal yAcc(t), inertial sensors measuring vibrations of Filter#1 (and the underlying chain) 'relative to the fixed stars' rather than to a noisy local reference, as in the case of the LVDT sensor.

Let's move on to examine the actual control part. Once the signal yLA(t) is constructed, the output signal, proportional to the force we want to apply to Filter#1, is derived by filtering with the 'yCfull' and 'intg' blocks. Their transfer functions and the product are illustrated in the following figure.

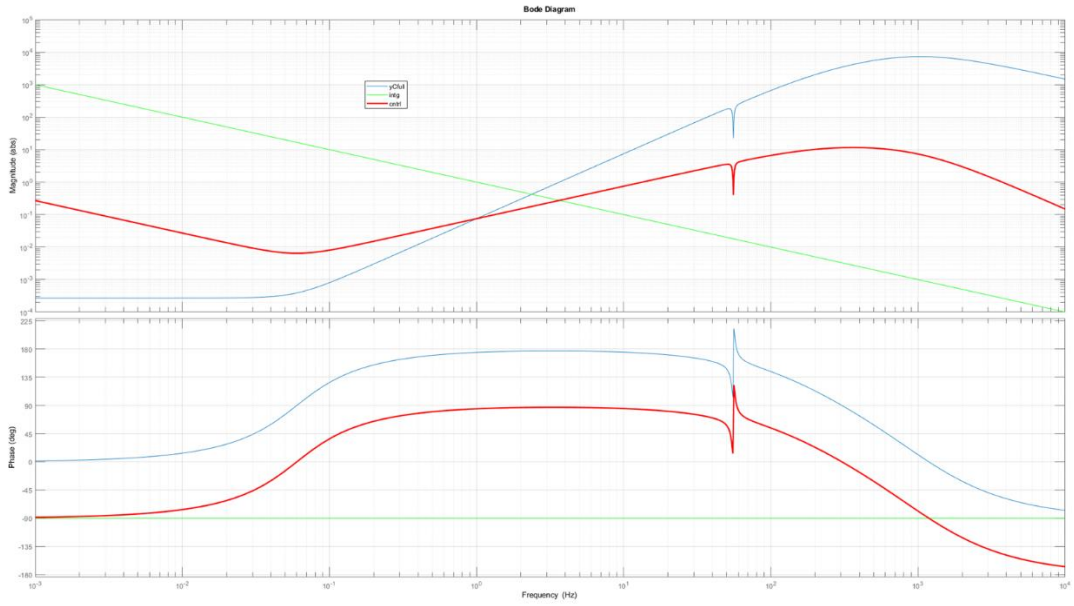


```
yCfull.flt
 Complex zeroes   frequency   0.06              Q       0.7
 Complex zeroes   frequency   55.66             Q       200
 Complex poles    frequency   55.66             Q       20
 Real     pole    frequency   200
 Real     poles   frequency   1000              Q       0.5
```

```
intg.flt
 Real     pole    frequency   0
```

The controller used is relatively simple. It essentially comprises an integrator (intg.flt) with a transfer function H(s) = 1/s, in series with a double differentiator featuring a complex zero pair at 0.06 Hz. The double zero-double pole pair at 55.66 Hz introduces a notch filter at 55.66 Hz, and three more poles at higher frequencies. Observing the trend of the red curve resulting from the two filters, we can speculate on the frequency chosen for unity gain, presumed to be where the phase lead of the filter is more significant, approximately around 3 Hz. If this assumption is accurate, we can determine the value of the mechanical transfer function always around 3 Hz. Specifically, if the open-loop gain magnitude should be 1 at 3 Hz, the magnitude of the mechanical transfer function at 3 Hz should be 1 / [Abs(yCfull) * Abs(intg)], approximately 1/0.23 = 4.35. In this case, the mechanical transfer function having yCorr(t) as input and yLA(t) as output. The units of this transfer function are not in meters per Newton but are arbitrary units since we are not concerned with the calibration factors of both the yLA and yCorr signals.

Mechanical Transfer Function

As we've seen, we have at least one point in the mechanical transfer function. Let's consider how to add further points without calculating the Lagrangian. We know that the lowest-frequency vertical mode is at approximately 100 mHz [RD10]. If I apply a force to Filter #1 and measure its position, the maximum phase shift between force and displacement cannot exceed 180 degrees[2]. Starting from zero frequency, the mechanical transfer function will exhibit an initial resonance peak around 100 mHz before asymptotically decreasing as $1/f^2$. The presence of other cascaded filters will introduce a series of double zero-double pole pairs.

We anticipate something akin to what's depicted in the following figure, where the choice of resonance frequencies and their quality factors is entirely arbitrary (as we've seen, these frequencies were not utilized for controller sizing). What matters is that the mechanical transfer function maintains a phase always between 0 and 180 degrees.

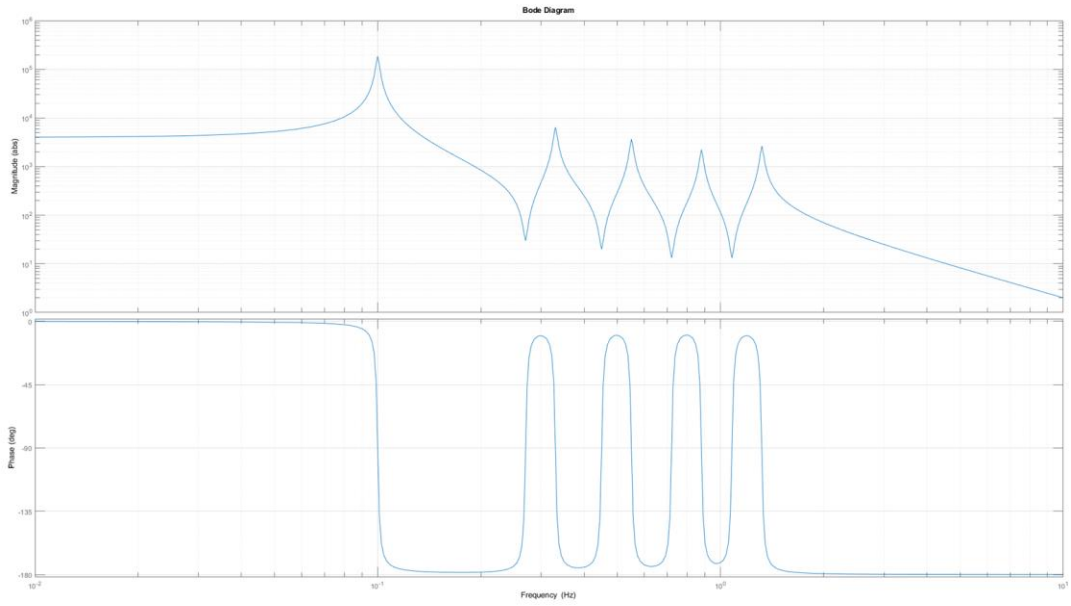

[2] **In our research group we always mention this feature as the "Luciano's Theorem" (after colleague Luciano Di Fiore). Actually, in addition of being quite intuitive thinking that force per velocity is absorbed power and cannot be negative, the demonstration comes from W. Cauer (1900-1945), applied to the study of electrical impedances,**

The overall loop gain is determined by the product of the mechanical transfer function and the controller, as depicted in the following figure. As observed, the phase response, where the magnitude is greater than one, remains far from 180 degrees, ensuring the stability of the closed-loop system. As expected, the presence of the filters in the chain does not influence the system's stability in any way. However, as we'll explore later, their presence affects the behavior of the closed-loop system.

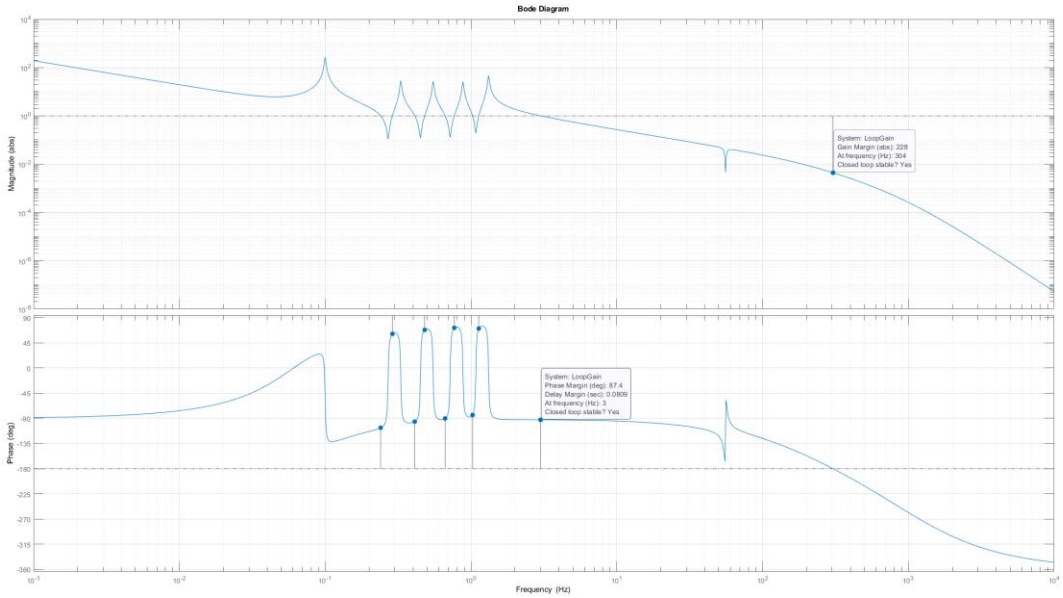

Closing The Loop

Now, we aim to observe the transformation of the mechanical transfer function yLa/yCorr when the feedback loop is closed. However, to achieve this, we need to create a new Simulink diagram to highlight the closed-loop behavior of the chain of mechanical filters and the outputs of the LVDT sensor and accelerometers.
In the following diagram, I have included the LTI blocks seen previously with two additions. The Deriv2 block implements a simple transfer function with two zeros at the origin and two poles at 1000 rad/sec to derive an acceleration signal from the position measurement y1. The second inserted block is Hmech, which implements the transfer function for vertical seismic noise. Assuming linearity of the entire system, we can consider that the vertical displacement of Filter #1 is a result of the combined contributions of the force acting on the filter and the seismic ground noise filtered by the mechanical transfer function Hmech. Hmech and Gmech follow the same pattern, differing only in the value of the low frequency response, proportional to 1/k for Gmech and 1 for Hmech.

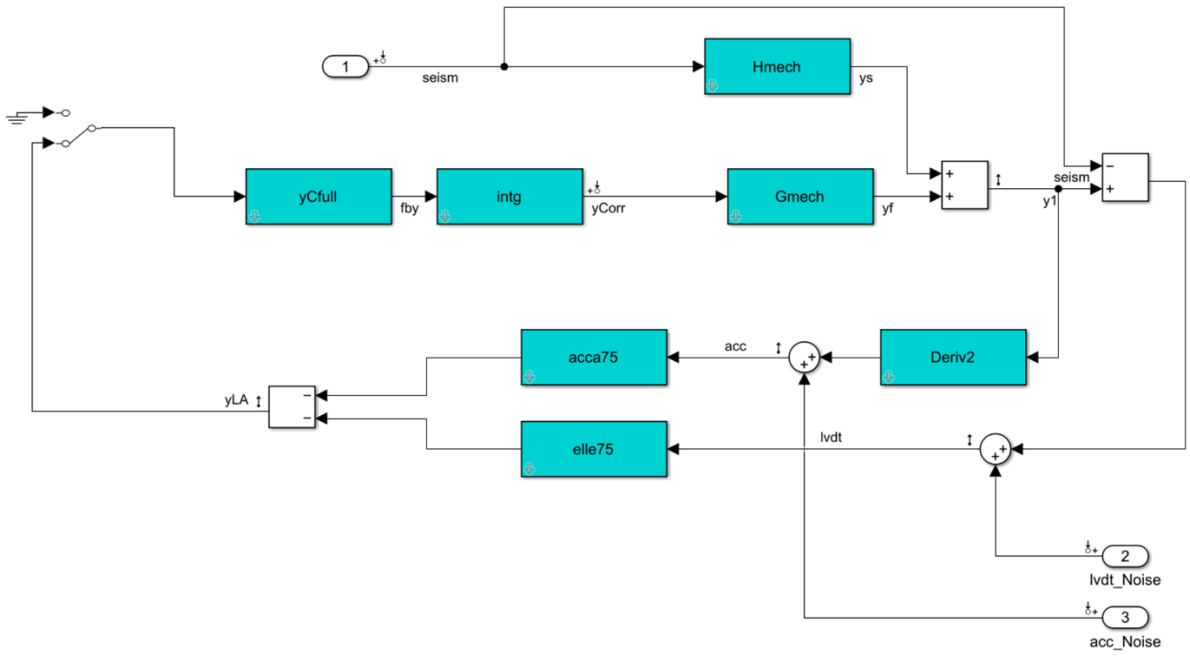

The closed-loop response compared to the open-loop response is depicted in the following figure. It's evident that in the transfer function between the applied force and y1, which is the displacement of Filter #1, there is gain from low frequencies up to the unity gain frequency. However, examining the vertical seismic transfer function, we notice that the gain is restricted to the range where the correction signal is derived from the accelerometer sensor, above the 75 mHz cross frequency of complementary filters elle75 and acca75.

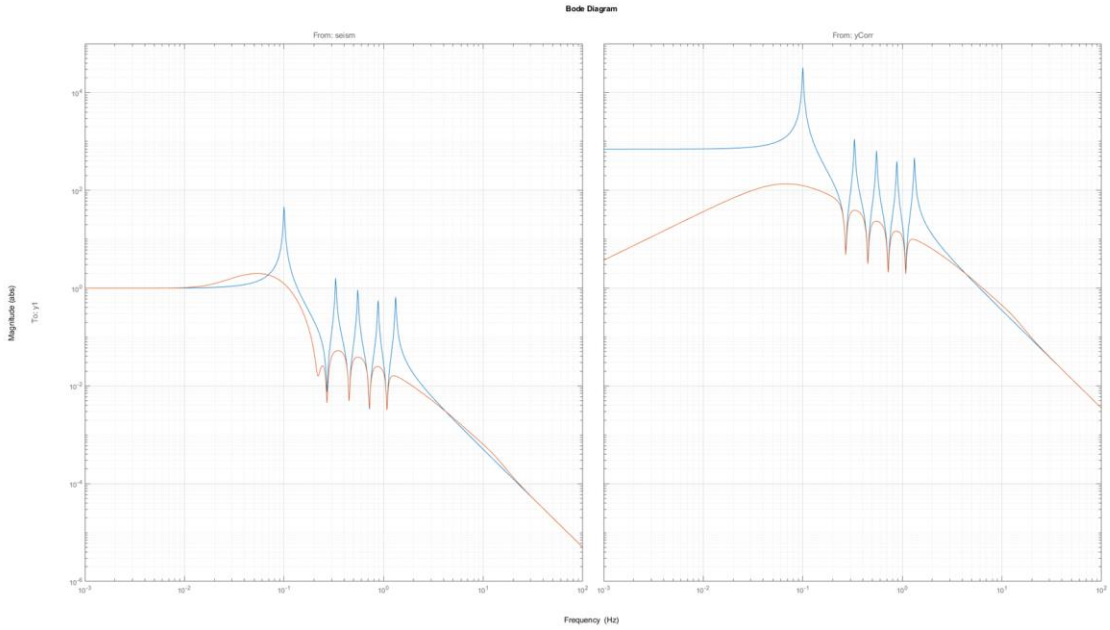

Noise Transfer Functions

In the following picture we report the transfer functions between respectively, vertical seism, correction signal, accelerometer noise, lvdt noise and the Filter#1 displacement. Of course, accelerometer and LVDT noise contribution is shown only for the closed loop case.

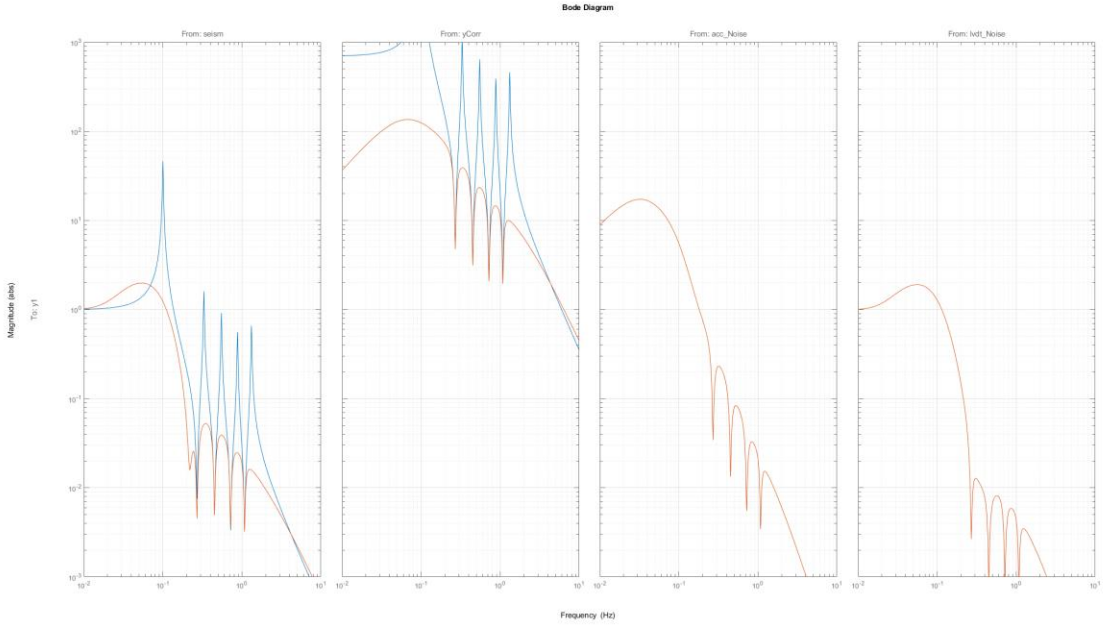

Wasn’t it a Digital Control System?

Throughout our analysis, we've treated the system as continuous-time. We've disregarded signal sampling effects and processor-induced delays. However, we can retrospectively estimate the impact of using a digital controller. Assuming τ = 200 us as maximum total delay between input and output of our digital controller, that is two complete cycles at 10 kHz due to pipeline between processors taking care of signals readout and processor computing and applying the correction forces, we have a phase shift equal to $-2 \pi f \tau$. Below 10 Hz we have a phase shift less than 1 degree, small enough to be negligible in our stability studies. The use of double precision floating point calculation and transformation of filters into second order cascaded sections, guarantees a negligible contribution from arithmetic noise. Finally, signals quantization was not considered. It is supposed to add up to sensors and actuators noise whose study was not within the scope of this document.

.

References

[RD1] Kailath,T. (1980). Linear systems. Prentice-Hall.

[RD2] Ogata,K. (2010).Modern Control Engineering 5th ed.UK:Prentice Hall.

[RD3] https://en.wikipedia.org/wiki/Reverse_engineering

[RD4] A. Gennai, T. Maiani, S. Mancini, D. Passuello, R. Taddei, A Control Model For The Inverted Pendulum", VIR-NOT-PIS-1390-101, May 21st, 1997

[RD5] R. Del Fabbro, A. Di Virgilio, A. Giazotto, H. Kautzky, V. Montelatici, D. Passuello,Three-dimensional seismic super-attenuator for low frequency gravitational wave detection, Physics Letters A,Volume 124, Issues 4–5, 1987, Pages 253-257, ISSN 0375-9601,https://doi.org/10.1016/0375-9601(87)90632-3.

[RD6] M. Beccaria, M. Bernardini, E. Bougleux, S. Braccini, C. Bradaschia, C. Casciano, G. Cella, E. Cuoco, E. D'Ambrosio, G. De Carolis, R. Del Fabbro, R. De Salvo, A. Di Virgilio, I. Ferrante, F. Fidecaro, R. Flaminio, A. Gaddi, A. Gennai, G. Gennaro, A. Giazotto, L. Holloway, P. La Penna, G. Losurdo, S. Malik, S. Mancini, J. Nicolas, F. Palla, H.B. Pan, F. Paoletti, A. Pasqualetti, D. Passuello, R. Poggiani, P. Popolizio, F. Raffaelli, A. Vicere, F. Waharte, Z. Zhang, Extending the VIRGO gravitational wave detection band down to a few Hz: metal blade springs and magnetic antisprings, Nuclear Instruments and Methods in Physics Research Section A: Accelerators, Spectrometers, Detectors and Associated Equipment, Volume 394, Issue 3, 1997, Pages 397-408,ISSN 0168-9002,https://doi.org/10.1016/S0168-9002(97)00661-X.

[RD7] https://www.picmg.org/openstandards/microtca/

[RD8] Peter R. Saulson; Vibration isolation for broadband gravitational wave antennas. Rev. Sci. Instrum. 1 August 1984; 55 (8): 1315–1320. https://doi.org/10.1063/1.1137923

[RD9] Alberto Gennai, VIR-SPE-PIS-4900-129, VIRGO DSP System Short User Manual June 26th, 2004.

[RD10] Paolo Ruggi, Inertial control of SR suspension vertical top stage, using the chain elongation as an accelerometer. July 31st 2020, VIR-0692A-20 LKV

oOo